



# A coupled adsorption–aggregation model of the POC/<sup>234</sup>Th ratio of marine particles

Adrian B. Burd<sup>a,\*</sup>, S.B. Moran<sup>b</sup>, George A. Jackson<sup>a</sup>

<sup>a</sup>*Department of Oceanography, Texas A & M University, College Station, TX 77840-3146, USA*

<sup>b</sup>*Graduate School of Oceanography, University of Rhode Island, Narragansett, RI 02882-1197, USA*

Received 28 August 1998; received in revised form 22 February 1999; accepted 23 February 1999

---

## Abstract

Thorium has been frequently used as a tracer of particulate carbon removal from the ocean surface mixed layers. Although coagulation is known to be important in the process, models used to interpret measurements have been limited to simple descriptions of coagulation. We present results from a coupled adsorption–aggregation model for <sup>234</sup>Th scavenging. The aggregation component models the particle size spectrum from colloidal particles to particles of about 100 μm in size and incorporates details of the physical mechanisms that bring particles together. We make comparisons between an adsorption model that has a constant mass specific adsorption rate and one that is purely transport limited, the former of which is shown to be unphysical for larger particles. The combined model reproduces the observed inverse dependence of POC/<sup>234</sup>Th on particle size. Comparison with observational results is made by simulating a series of filtrations using the model results. The filtered values are determined by the maximum of the particle distribution within the relevant size range, and consequently affect the comparison between observed values and model output. This stresses the importance of the particle size spectrum in the scavenging process and suggests that measurements using more particle size classes should be made to accurately determine kinetic rates. © 1999 Elsevier Science Ltd. All rights reserved.

*Keywords:* Trace metal scavenging model; Thorium; POC flux

---

## 1. Introduction

The ability to accurately estimate the vertical flux of organic carbon from the upper ocean is important for understanding the global carbon budget. The dominant

---

\* Corresponding author. Fax: 001-409-847-8879.

E-mail address: adrian@plankton.tamu.edu (A.B. Burd)

sources of particulate organic carbon (POC) are ultimately biological. The downward flux of this material results from the sinking of particles from the surface mixed layer. The rate at which these particles sink (and hence the value of the POC flux) depends upon the particle size distribution, and hence on the dynamics of particle aggregation.

The radio-isotope  $^{234}\text{Th}$  ( $t_{1/2} = 24.1$  days) has been used as a tracer to estimate upper ocean POC export (Buesseler et al., 1992,1995; Cochran et al., 1994; Bacon et al., 1996; Murray et al., 1996; Moran et al., 1997) Thorium is very particle active and the disequilibrium between  $^{234}\text{Th}$  and  $^{238}\text{U}$  in the mixed layer provides a quantitative measure of the export of  $^{234}\text{Th}$  on time-scales of several days to months. To derive POC fluxes from  $^{234}\text{Th}$  tracer distributions requires information on the  $\text{POC}/^{234}\text{Th}$  ratio of sinking particles, typically obtained by direct measurement.

The  $\text{POC}/^{234}\text{Th}$  ratio of marine particles can vary significantly in space and time due to changes in, for example, biological productivity, particle export and particle size distribution (Moran et al., 1993; Buesseler et al., 1995). Furthermore, the average of the  $\text{POC}/^{234}\text{Th}$  ratio on sinking particles is not the same as that on suspended material (Moran et al., 1993). Developing a quantitative understanding of the processes causing natural variability in  $\text{POC}/^{234}\text{Th}$  ratios of marine particles is essential for validating the use of  $^{234}\text{Th}$  to estimate POC export fluxes from the surface ocean.

Compilation of the  $\text{POC}/^{234}\text{Th}$  ratio in several particle size classes shows this ratio to decrease with particle size (Moran et al., 1993). Previous studies have suggested that this could be explained by the preferential remineralization of POC via biological processes (Moran et al., 1993; Buesseler et al., 1995). More recent studies have shown that  $\text{POC}/^{234}\text{Th}$  ratios can increase with particle size (Niven et al., 1995; Buesseler et al., 1996; Charette and Moran, 1999; Charette et al., 1999). An increase in the  $\text{POC}/^{234}\text{Th}$  ratio with particle size has been attributed to a decrease in the cell surface area : volume ratio during cell growth (Moran et al., 1993) and in some cases where increasing ratios have been found, the samples contained an abundance of large ( $\sim 200 \mu\text{m}$ ) diatoms or aggregates (Charette and Moran, 1999; Charette et al., 1999). Biological processes are also expected to play an important role in affecting the regional and temporal variability of the  $\text{POC}/^{234}\text{Th}$  ratio of marine particles.

Many processes contribute to thorium scavenging. These include chemical adsorption and de-adsorption of thorium onto particles, particle sinking and particle aggregation. Existing models (e.g., Clegg and Whitfield, 1993) of thorium scavenging recognize that these processes depend on particle size by including two particle size classes representing suspended and settling particles. Such models often use simplified kinetics to represent the flows between these particle classes. For example, the flow from suspended to settling particles resulting from aggregation is usually represented as a first-order process. However, it is known that particle aggregation is a second-order process, described by a different rate expression (Pruppacher and Klett, 1980).

More sophisticated models of particle aggregation have been incorporated into thorium scavenging models. Honeyman and Santschi (1989) described the aggregation of colloidal particles using an aggregation model developed by Farley and Morel (1986). This latter model was developed to describe a batch reactor system and thus has no source of particulate material. In addition, it describes the aggregation of spherical particles having a density that is independent of the particle size. For these

reasons, the Farley and Morel aggregation model is of limited use for describing aggregation of marine particles. The Honeyman and Santschi model (the Brownian pumping model) (1989) uses the Farley and Morel model (1986) to argue that the aggregation of colloidal material is the rate determining kinetic step for the scavenging of trace metals in natural aquatic systems. The Brownian pumping model suffers from the same limitations as the Farley and Morel aggregation model and in addition does not include the aggregation of colloidal particles into larger, settling particles. The Farley and Morel model has recently been extended to include improved formulations of the particle encounter rate as well as a fractal description of particle shape (Burd and Jackson, 1997). This extended model forms the basis of the model employed here.

In this paper we present results from a coupled aggregation/adsorption model of thorium scavenging that includes a dynamic description of aggregation and adsorption as functions of particle size. Because the rates of both aggregation and trace metal adsorption depend on particle size, the model calculates the particle size spectrum over a wide range of particle sizes ( $\sim 1$  nm to  $\sim 100$   $\mu$ m). The model concentrates on the particle kinetics, for which there exists a well developed theory. We compare the model results for the POC/ $^{234}\text{Th}$  ratio with a compilation of data covering a wide range of systems from open ocean to coastal waters (Moran et al., 1993). The model simulations provide a quantitative basis for interpreting the  $^{234}\text{Th}$ -derived POC fluxes that includes chemical adsorption and particle dynamics. Our analysis indicates that a physical adsorption–aggregation model can reproduce the observed inverse dependence of the POC/ $^{234}\text{Th}$  ratio on particle size.

## 2. Data sets

Size fractionated POC/ $^{234}\text{Th}$  data were compiled from the literature and published field data from the upper water column. Data were obtained from the NABE (Buesseler et al., 1992), EqPac (Bacon et al., 1996), VERTEX 2, VERTEX 4 projects (Coale and Bruland, 1987; Bruland, unpublished data) and from BATS-32 (Moran and Buesseler, 1992), The Gulf of Mexico (Baskaran et al., 1992) and a spring phytoplankton bloom in Bedford Basin, N.S., Canada (Niven et al., 1995) (Fig. 1). Several filter sizes, including 56, 0.7, 0.2  $\mu$ m, were used in the various data sets. The observed size-fractionated POC/ $^{234}\text{Th}$  ratios from the various locations consistently decreased with increasing particle size (Fig. 1). The observed dependence between POC/ $^{234}\text{Th}$  and particle size and the regional variability in POC/ $^{234}\text{Th}$  ratios may be a function of the magnitude of particle export, particle aggregation and disaggregation, and food-web dynamics (Moran et al., 1993; Buesseler et al., 1995). For example, the bloom conditions during the NABE experiment were characterized by high particle export, low recycling and relatively high POC/ $^{234}\text{Th}$  for whole bottle particulate samples (Buesseler et al., 1992). By contrast, the low export production and high remineralization rates in the EqPac experiment resulted in lower POC/ $^{234}\text{Th}$  (Buesseler et al., 1995; Bacon et al., 1996; Murray et al., 1996).

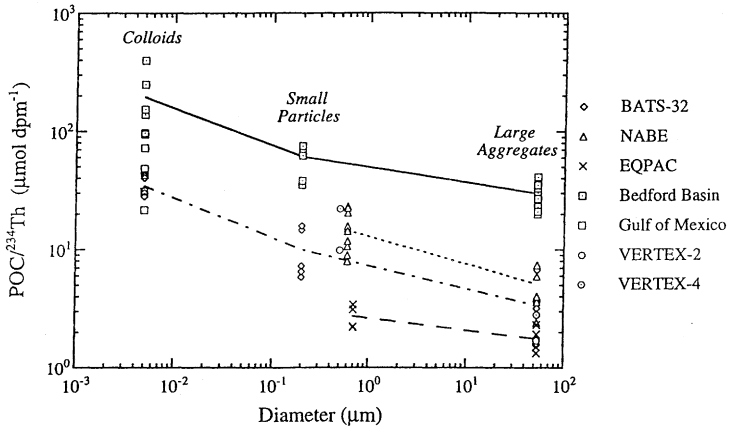


Fig. 1. POC/ $^{234}\text{Th}$  ratios as a function of particle size from the upper ocean. The POC/ $^{234}\text{Th}$  ratios shown are for the filter sizes and larger particles. The colloidal size range is defined here as between 10,000 NMW (nominal molecular weight) cross-flow filtration filters and 0.2–0.4  $\mu\text{m}$ . Small particles (0.2–1  $\mu\text{m}$ ) were collected using either GF/F glass-fiber filters (0.7  $\mu\text{m}$ ), micro-quartz filters (1  $\mu\text{m}$ ), Gelman Mini-Capsule filters (0.2  $\mu\text{m}$ ), or Nuclepore filters (0.2  $\mu\text{m}$ , 0.4  $\mu\text{m}$ ). Large aggregates were collected using 53  $\mu\text{m}$  Nitex screens or sediment traps. Sediment traps were used to collect sinking particles in the NABE and Bedford Basin experiments. Data from: NABE (Buesseler et al., 1992); EqPac (Bacon et al., 1996); VERTEX 2, VERTEX 4 projects (Coale and Bruland, 1987; Bruland, unpublished data); BATS-32 (Moran and Buesseler, 1992); Gulf of Mexico (Baskaran et al., 1992); Bedford Basin (Niven et al., 1995).

### 3. The models

The coupled aggregation/adsorption model (Fig. 2) we used builds on the Brownian pumping model developed by Honeyman and Santschi (1989) and a steady-state version of the aggregation model used by Burd and Jackson (1997). Marine particles vary in size from the colloidal (having radius  $r \sim 1 \text{ nm}$ ) to those easily seen by divers (1 mm or larger). Mass transport arguments imply that trace metals adsorb preferentially onto the colloidal particles. The vertical flux of material from the mixed layer, on the other hand, is dominated by larger particles.

#### 3.1. The particle coagulation model

The coagulation model simulates the particle size distribution resulting from the collision and subsequent sticking together of particles over a wide range of particle sizes. The particle size distribution is conveniently represented in terms of the particle size spectrum,  $n(m)$ . This is defined such that if  $N(m)$  is the cumulative particle concentration (i.e., the number concentration of particles having mass greater than  $m$ ), then

$$n(m) = -\frac{dN(m)}{dm}. \quad (1)$$

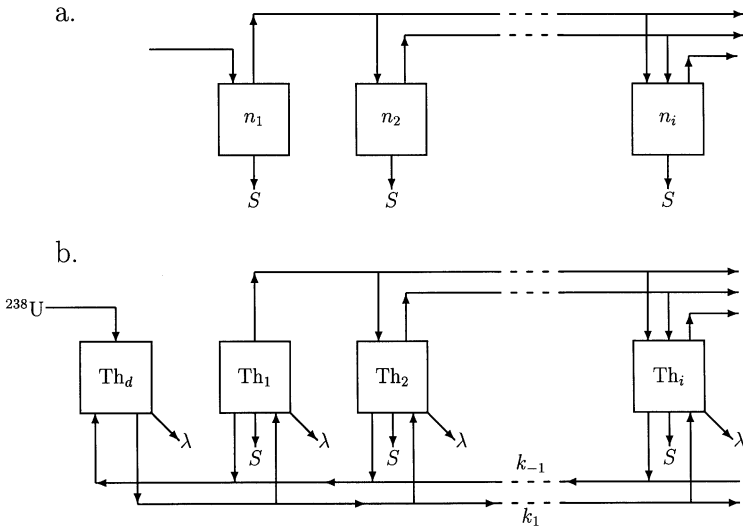


Fig. 2. (a) Schematic of the coagulation model. Particles are input into the first section ( $n_1$ ). Aggregation (as shown by the arrows on top of the boxes) occurs between all particle size classes. Losses from sinking ( $S$ ) can occur for all particles. (b) Schematic of the thorium adsorption model. Thorium enters into the dissolved compartment  $Th_d$  through decay of  $^{238}U$ . Adsorption ( $k_1$ ) and desorption ( $k_{-1}$ ) occur between  $Th_d$  and all particle size classes. Thorium decay ( $\lambda$ ) and settling losses ( $S$ ) occur for all particles.

Particle mass is a useful measure of particle size to use in coagulation calculations because mass is conserved when two particles collide. However, particle collision frequencies are best expressed in terms of particle radius. In addition, observations of particle concentrations are frequently made in terms of particle radius. The conversion between  $n$  calculated as a function of mass and  $n$  calculated as a function of radius is straightforward, because the particle size spectrum can be expressed as a function of any measure of particle size. For example, the particle size spectrum in terms of particle radius is given by

$$n(r) = -\frac{dN(r)}{dr} = \frac{dm}{dr} n(m). \tag{2}$$

Classical coagulation theory yields an integro-differential equation describing the evolution of  $n$  in a well mixed layer of thickness  $Z$  (Pruppacher and Klett, 1980; Jackson and Lochmann, 1992)

$$\begin{aligned} \frac{dn(m, t)}{dt} = & \frac{\alpha}{2} \int_0^m \beta(m_1, m - m_1) n(m_1, t) n(m - m_1, t) dm_1 \\ & - \alpha n(m, t) \int_0^\infty \beta(m, m_1) n(m_1, t) dm_1 \\ & - \frac{w(m)}{Z} n(m, t) + \mu(m), \end{aligned} \tag{3}$$

where  $\beta(m, m_1)$ , the coagulation kernel, provides the probabilities for collision between particles with masses  $m$  and  $m_1$ ,  $\alpha(m, m_1)$  is the probability that the two particles stick once they have collided,  $w$  is the particle settling velocity,  $\mu$  the particle input rate. The first term in equation Eq. (3) is the rate at which collisions form new particles with masses lying between  $m$  and  $m + dm$ , the second term is the rate at which particles are lost from the same mass interval through coagulation. The third term is the rate at which particles sink out of a well-mixed layer and the final term represents a size-dependent particle input.

Since Eq. (3) is expressed in terms of particle mass and the coagulation kernel is in terms of particle radius, we need a relationship between the mass and radius of an aggregate. Particles formed by coagulation have a porosity that increases with particle size. This can be described using a fractal scaling (Vicsek, 1992) and has been observed in marine aggregates (Logan and Wilkinson, 1990). We can model an aggregate as an object composed of identical spherical sub-particles, each having a mass  $m_0$  and a radius  $a_0$ . The mass,  $m$ , of the aggregate is then related to a characteristic radius by

$$\frac{m}{m_0} = \left( \frac{r}{a_0} \right)^{D_f}, \quad (4)$$

where  $D_f$  is the cluster fractal dimension. If  $D_f = 3$  then (4) expresses the familiar relationship between the radius and mass of a solid sphere; values of  $D_f > 3$  are not physically realizable. Particles for which  $D_f < 3$  are called fractals, and their properties differ from solid particles. For example, the mean density of a fractal aggregate decreases as the size of the aggregate increases. This arises from the fact that the porosity of the fractal aggregate is not uniform but instead increases as one moves out from the center of the particle (Smirnov, 1990). Fractal dimensions of marine aggregates have been measured, and results lie between 1.3 and 3.75 (Logan and Wilkinson, 1990; Jiang and Logan, 1991; Li and Logan, 1995; Jackson et al., 1997), values of  $D_f > 3$  presumably arising from measurement error. A value of  $D_f = 2.6$  was chosen to maintain consistency with previous numerical simulations (Burd and Jackson, 1997). The characteristic aggregate size given in (4) can be related to other measures of aggregate size, such as the radius of gyration (Jackson, 1995), which was used in the simulations presented here.

The first step in solving Eq. (3) is the formulation of the coagulation kernels,  $\beta$ , in terms of variables that characterize the particles. Standard treatments of coagulation use three mechanisms for bringing particles together: Brownian motion, shear (both turbulent and laminar) and differential sedimentation. These are assumed to act independently so that the total coagulation kernel can be written

$$\beta(r_i, r_j) = \beta_{\text{Br}}(r_i, r_j) + \beta_{\text{sh}}(r_i, r_j) + \beta_{\text{ds}}(r_i, r_j) \quad (5)$$

where the subscripts Br, sh, and ds denote the different mechanisms, and  $r_i$  and  $r_j$  are the particle radii.

Two approaches to formulating the coagulation kernel are often used (e.g., Pruppacher and Klett, 1980). The rectilinear formulation ignores any hydrodynamic interaction between the colliding particles. In this case the particle collision rate can

be calculated using the geometric cross-sections of the particles. The curvilinear formulation takes hydrodynamic interactions into account and results in smaller particle collision rates. Experimental measurements of collision frequencies between fractal aggregates and small particles give values that lie between those expected for pure rectilinear and pure curvilinear coagulation (Li and Logan, 1997a,b). The results in this paper are shown for the rectilinear case and so may over-estimate the aggregation rates between dissimilar sized particles. The coagulation kernels for Brownian motion, shear and differential sedimentation between two particles having radii  $r_i$  and  $r_j$  are (Pruppacher and Klett, 1980):

$$\beta_{Br}(r_i, r_j) = 4\pi(D_i + D_j)(r_i + r_j), \tag{6}$$

$$\beta_{sh}(r_i, r_j) = \frac{4}{3}\gamma(r_i + r_j)^3, \tag{7}$$

$$\beta_{ds}(r_i, r_j) = \pi(r_i + r_j)^2|w_j - w_i|, \tag{8}$$

where  $D_i = kT(6\pi\mu r_i)^{-1}$  is the diffusion coefficient for particle  $i$ ,  $k$  is Boltzmann's constant,  $T$  is the absolute temperature,  $\gamma$  is the fluid shear rate,  $\mu$  is the dynamic viscosity of water and  $w_i$  and  $w_j$  are the settling velocities of the particles  $i$  and  $j$ .

The fractal nature of the aggregates expressed in (4) affects estimates of aggregation rates. The values of the coagulation kernels change for porous particles, because settling rates are functions of particle radii (which increase through aggregation) and particle densities (which decrease through aggregation relative to the values for solid particles). Using a fractal density therefore affects the differential sedimentation and shear kernels by changing both the settling velocity and the interaction distances.

The coagulation equation Eq. (3) does not in general admit any analytical solutions (Drake, 1972). A numerical solution of the equation is made simpler by using a sectional approach (Gelbard et al., 1980; Jackson and Lochmann, 1992). For this, the range of particle sizes being considered is divided into contiguous size classes (sections) such that the particle mass at the upper bound of a section is twice that at its lower bound. The particle number spectrum is assumed to be separable into a factor that varies with time and another varying with particle size

$$n(m, t) = \frac{Q_l(t)}{mm_{l-1}}, \tag{9}$$

where the particle mass  $m$  lies between the upper,  $m_l$ , and lower,  $m_{l-1}$ , bounds on the section  $l$ , and  $Q_l$  is the total concentration of particulate mass of particles having  $m_l > m > m_{l-1}$ . Jackson and Lochmann (1992) modified the formulation given by Gelbard et al. (1980) to show that using (9) in (3) results in

$$\begin{aligned} \frac{dQ_l}{dt} = & \frac{\alpha}{2} \sum_{i=1}^{l-1} \sum_{j=1}^{l-1} {}^1\bar{\beta}_{i,j} Q_i Q_j - \alpha Q_l \sum_{i=1}^{l-1} {}^2\bar{\beta}_{i,l} Q_i - \frac{\alpha}{2} {}^3\bar{\beta}_{l,l} Q_l^2 - \alpha Q_l \sum_{i=l+1}^s {}^4\bar{\beta}_{i,l} Q_i \\ & - \frac{Q_l}{Zm_l} \int_{m_{l-1}}^{m_l} w(m) dm + \mu_i, \end{aligned} \tag{10}$$

where  $s$  is the total number of sections used in the simulation. Here  ${}^1\bar{\beta}_{i,j}$ ,  ${}^2\bar{\beta}_{i,l}$ ,  ${}^3\bar{\beta}_{l,l}$ , and  ${}^4\bar{\beta}_{i,l}$  are the sectional coagulation coefficients defined by Gelbard et al. (1980).

These are obtained by integrating the coagulation kernel (5) over relevant sections. The four different  $\bar{\beta}$  incorporate the frequency of collisions between particles in various sections. For example,  ${}^3\bar{\beta}_{l,l}$  represents the coagulation kernel for collisions between particles in section  $l$  with other particles in the same section, integrated over section  $l$ . These quantities are used to simplify the numerical scheme for solving the coagulation equation. The particle input rate,  $\mu_i$ , was chosen such that the only source of particles was into the size class containing the smallest particles.

The settling velocity of the aggregates was derived from the Stokes expression

$$w = \frac{2}{9} \frac{g (\rho_{ag} - \rho_w)}{v \rho_w} r^2. \quad (11)$$

The average density of the aggregate can be written

$$\rho_{ag} = \frac{v\rho_0 + (V - v)\rho_w}{V} = (1 - e)\rho_0 + e\rho_w, \quad (12)$$

where  $v = m/\rho_0$  is the volume of the solid material making up the aggregate,  $V$  is the volume of the sphere enclosing the aggregate, and  $e$  is the porosity. Eqs. (4), (11) and (12) combine to give

$$w(m) = \frac{g}{6\pi v \kappa} \left( \frac{1}{\rho_w} - \frac{1}{\rho_0} \right) m^{1-1/D_t}, \quad (13)$$

where  $\kappa = a_{0t}^D/m_0$ . A conversion factor of  $0.4 \text{ gC g}^{-1}$  (Peters, 1983) was used to convert particulate mass obtained from the model to organic carbon.

### 3.2. The tracer model

We wish to follow the amount of thorium adsorbed onto particles as those particles aggregate and settle out of the mixed layer. For each range of particle masses we need to keep track of the thorium that is adsorbed onto the particles in that mass range, the thorium that desorbs from those particles and the adsorbed thorium that decays. We also need to follow the particulate thorium that is carried into other particle mass ranges by coagulation.

An equation analogous to (3) can be written down for the thorium activity on particulate material

$$\begin{aligned} \frac{d\text{Th}(m, t)}{dt} = & \frac{\alpha}{2} \int_0^m (\text{Th}(m_1) + \text{Th}(m - m_1)) \beta(m_1, m - m_1) n(m_1, t) n(m - m_1) dm_1 \\ & - \alpha n(m) \int_0^\infty (\text{Th}(m) + \text{Th}(m_1)) \beta(m, m_1) n(m_1) dm_1 \\ & - \frac{w(m)}{Z} n(m) \text{Th}(m) - \lambda \text{Th}(m) - k_{-1} \text{Th}(m) + k_1(m) \text{Th}_d n(m) \end{aligned} \quad (14)$$

where the particle size spectrum,  $n(m)$ , is assumed to be in steady state,  $\text{Th}(m) dm$  is the thorium activity per unit volume contained on particles in the mass range  $m$  to

$m + dm$ ,  $\lambda$  is the  $^{234}\text{Th}$  decay rate, and  $k_1$  and  $k_{-1}$  are the thorium adsorption and desorption rate constants, respectively. The first term represents the rate at which thorium is brought into the particle mass range  $m$  to  $m + dm$  through particle collisions. The second term is the rate at which thorium is lost from the same mass range by particle coagulation. The rate at which thorium is carried out of the same mass range by sinking particles is given by the third term. The next two terms represent loss rate of thorium due to radioactive decay and desorption. The final term gives the rate at which dissolved thorium,  $\text{Th}_d$ , is adsorbed onto particles having mass in the range  $m$  to  $m + dm$ .

Applying the sectional approach to these equations gives, for the dissolved thorium

$$\frac{d\text{Th}_d}{dt} = P - \lambda\text{Th}_d - k_1\text{Th}_d \sum_{i=1}^n Q_i + k_{-1} \sum_{i=1}^n \text{Th}_i, \tag{15}$$

where  $P$  represents the formation of thorium from the decay of uranium, and for the particulate thorium in section  $k$

$$\begin{aligned} \frac{d\text{Th}_k}{dt} = & \alpha \sum_{i=1}^{k-2} \left( \frac{1}{2} \beta_{i,k} - {}^3\beta_{i,k-1} \right) Q_{k-1} \text{Th}_i + \alpha \sum_{i=1}^{k-2} {}^3\beta_{i,k-1} Q_i \text{Th}_{k-1} \\ & + \frac{\alpha_4}{2} \beta_{k-1,k-1} Q_{k-1} \text{Th}_{k-1} + \alpha \sum_{i=1}^{k-1} {}^2\beta_{i,k} Q_k \text{Th}_i - \frac{\alpha_4}{2} \beta_{k,k} Q_k \text{Th}_k \\ & - {}^3\beta_{i,k} Q_i \text{Th}_k - \sum_{i=k+1}^n {}^5\beta_{i,k} Q_i \text{Th}_k \\ & - \lambda\text{Th}_k - k_{-1} \text{Th}_k + k_1 \text{Th}_d Q_k - \frac{\text{Th}_k}{Z m_k} \int_{m_{k-1}}^{m_k} w(m) dm \end{aligned} \tag{16}$$

Eqs. (10), (15) and (16) form a set of coupled, non-linear ordinary differential equations. Because Eqs. (15) and (16) do not affect (10), the particle size spectrum can be found independently of the thorium distribution. The resulting values for the steady state mass distribution were then used as input for the numerical solution of (16)–(15).

The complete model was formed from Eqs. (10) (15) and (16), and forms a set of coupled, nonlinear ordinary differential equations. The relevant time-scales in the problem (e.g., coagulation rates, adsorption rates, settling rates) vary with particle size. A large range of relevant time-scales can lead to spurious numerical solutions, and such systems of equations are called stiff (Press et al., 1992). For this reason, the equations were integrated using a Bader–Deuffhard algorithm designed to deal with stiff systems (Press et al., 1992). The code was written in FORTRAN-77 and run on a DEC Alpha 3000 machine. Two sets of simulations were run, one representing an open ocean system ( $Z = 30 \text{ m}$ ,  $\mu = 0.01 \text{ mg L}^{-1} \text{ d}^{-1}$ ) and the other a shallow coastal system ( $Z = 3 \text{ m}$ ,  $\mu = 0.1 \text{ mg L}^{-1} \text{ d}^{-1}$ ). The value of the particle production rate in the open ocean was obtained from estimates of primary production, and similar values have been used in previous models (Clegg and Whitfield, 1990). The value of  $\mu$  for the coastal ocean was based on the open ocean model and the fact that estuarine primary productivities can be ten times those of the open ocean (Valiela, 1995). The

open ocean value of the mixed layer depth,  $Z$ , is within the range of shallow summer values (Mann and Lazier, 1991). A mixed layer depth of a few meters is typical in estuarine environments (Niven et al., 1995), with the value used here chosen for ease of conversion between the open ocean and estuarine cases.

### 3.3. The adsorption models

Models of trace metal adsorption onto marine particles vary in complexity (e.g., Bacon and Anderson, 1982; Clegg and Sarmiento, 1989). In this work we initially followed Clegg and Whitfield (1993) and assumed that thorium adsorption could be modeled with a pseudo rate constant that was constant for all particles (model A);

$$k_1^i = 2.68 \times 10^5 \text{ cm}^3 \text{ g}^{-1} \text{ d}^{-1} \quad (17)$$

for all sections  $i$  (Fig. 3). This assumes that the available surface site concentration per unit mass is constant as a function of particle size (Clegg and Whitfield, 1993). This model has been previously used to model thorium data from the JGOFS North Atlantic Bloom Experiment (Clegg and Whitfield, 1993).

Two other adsorption models were also examined. In model B, the adsorption rate constant was calculated by applying the sectional approximation to the standard equation for transport to a spherical particle (Clift et al., 1978). The resulting rate

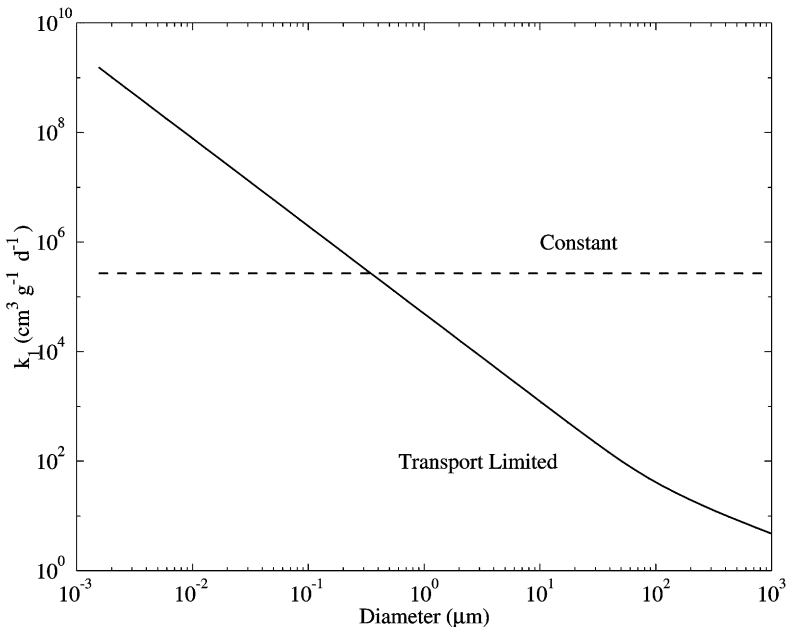


Fig. 3. Specific adsorption coefficient versus particle radius. The dashed line is the constant value used here and by Clegg et al. (1993). The curved line shows the specific adsorption coefficient predicted by transport limitation alone.

constant was

$$k_1^j = \frac{2\pi D_f D}{m_{j+1} - m_j} \int_{r_j}^{r_{j+1}} (1 + (1 + \text{Pe})^{1/3}) dr, \quad (18)$$

where  $m_j, r_j$  are the mass and radius of particles at the lower bound of section  $j$ , and  $\text{Pe}$  is the Peclet number (Clift et al., 1978). In the simulations, the Peclet number varied between  $1.5 \times 10^{-12}$  for particles with  $r = 1$  nm to 15 for particles with  $r = 100$   $\mu\text{m}$ .

We also performed simulations using a third adsorption model (model C) formulated such that for each particle size, the minimum of models A and B was used.

The thorium desorption rate constant used in all the simulations was  $k_{-1} = 0.0068 \text{ d}^{-1}$  (Clegg and Whitfield, 1993).

#### 4. Results

The output from the model for the shallow, estuarine simulation is shown in Fig. 4 (solid lines). Both POC (Fig. 4a) and  $^{234}\text{Th}$  activity (Fig. 4b) are indicative of coagulation. Both curves show broad maxima for particles in the size range 1–100  $\mu\text{m}$ . For colloidal particles, the increase in POC with particle size results from rapid coagulation by Brownian processes. Particles larger than 100  $\mu\text{m}$  rapidly settle out of the shallow layer giving a rapid fall off in POC for these larger particles. The thorium activity displays similar features, except that the slopes of the curves are steeper indicating preferential adsorption onto the colloidal particles. The stepped nature of the solid curves arises from dividing the particle mass range into sections; each horizontal part of the solid curve represents the value of interest in one section. The POC and  $^{234}\text{Th}$  activities were combined to obtain values for the  $\text{POC}/^{234}\text{Th}$  ratio (Fig. 4c).

The model predicts a  $\text{POC}/^{234}\text{Th}$  ratio that decreases with increasing particle size, up to diameters of approximately 10  $\mu\text{m}$ , after which it remains approximately constant (Fig. 5). For a mixed layer depth of 30 m and input rate of  $0.01 \text{ mg L}^{-1} \text{ d}^{-1}$  (Fig. 5a) the model overestimates the  $\text{POC}/^{234}\text{Th}$  ratio by more than two orders of magnitude for colloidal particles. For small particles (0.1–1.0  $\mu\text{m}$ ) the model results fall close to the observed range (depicted by the vertical bars). For larger particles, the model results fall within the observed range.

For very shallow mixed layers (3 m), such as those in shallow estuarine areas, with higher particle input rates ( $0.1 \text{ mg L}^{-1} \text{ d}^{-1}$ ), the model gives  $\text{POC}/^{234}\text{Th}$  values that are approximately an order of magnitude larger than those with deeper mixed layers (Fig. 5b).

#### 5. Discussion

The model predicts a decrease of the  $\text{POC}/^{234}\text{Th}$  ratio with increasing particle size (Fig. 5). Model predictions of the  $\text{POC}/^{234}\text{Th}$  ratio for the colloidal particles are as

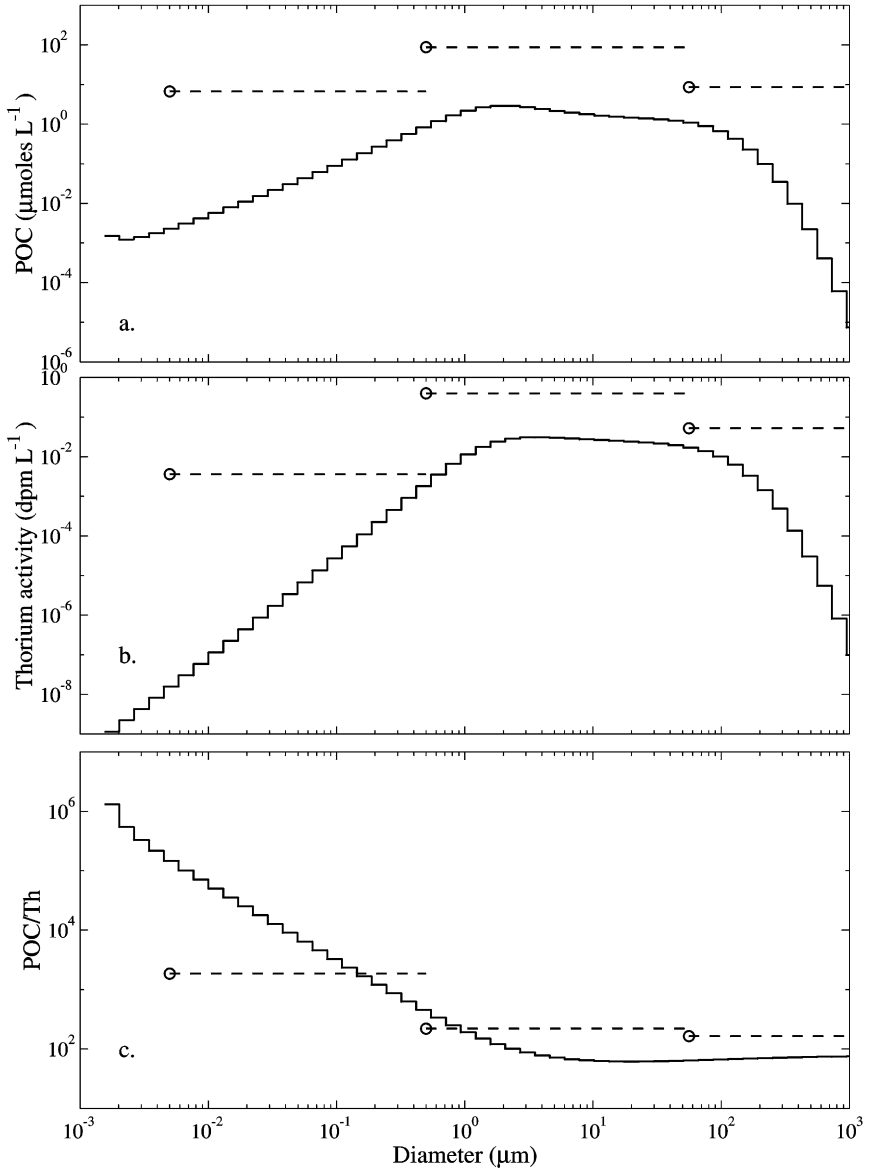


Fig. 4. Model results from a simulation using  $Z = 3$  m and particle input rate of  $0.1 \text{ mg l}^{-1} \text{ d}^{-1}$  demonstrating the effects of filtration. The model (solid lines) estimates the particulate organic carbon concentration (a) and thorium activity (b) within each section. To compare the observations with the model output, three coarse particle size classes were chosen:  $> 56 \mu\text{m}$  (large particles),  $0.5\text{--}56 \mu\text{m}$  (small particles) and  $< 0.5 \mu\text{m}$  (colloids). These size ranges are depicted by the horizontal dashed lines. The sectional distributions of POC and  $^{234}\text{Th}$  within each of these coarse ranges were summed up and the resulting values plotted as open circles. These values were then used to calculate the POC/ $^{234}\text{Th}$  ratio shown by the open circles in (c).

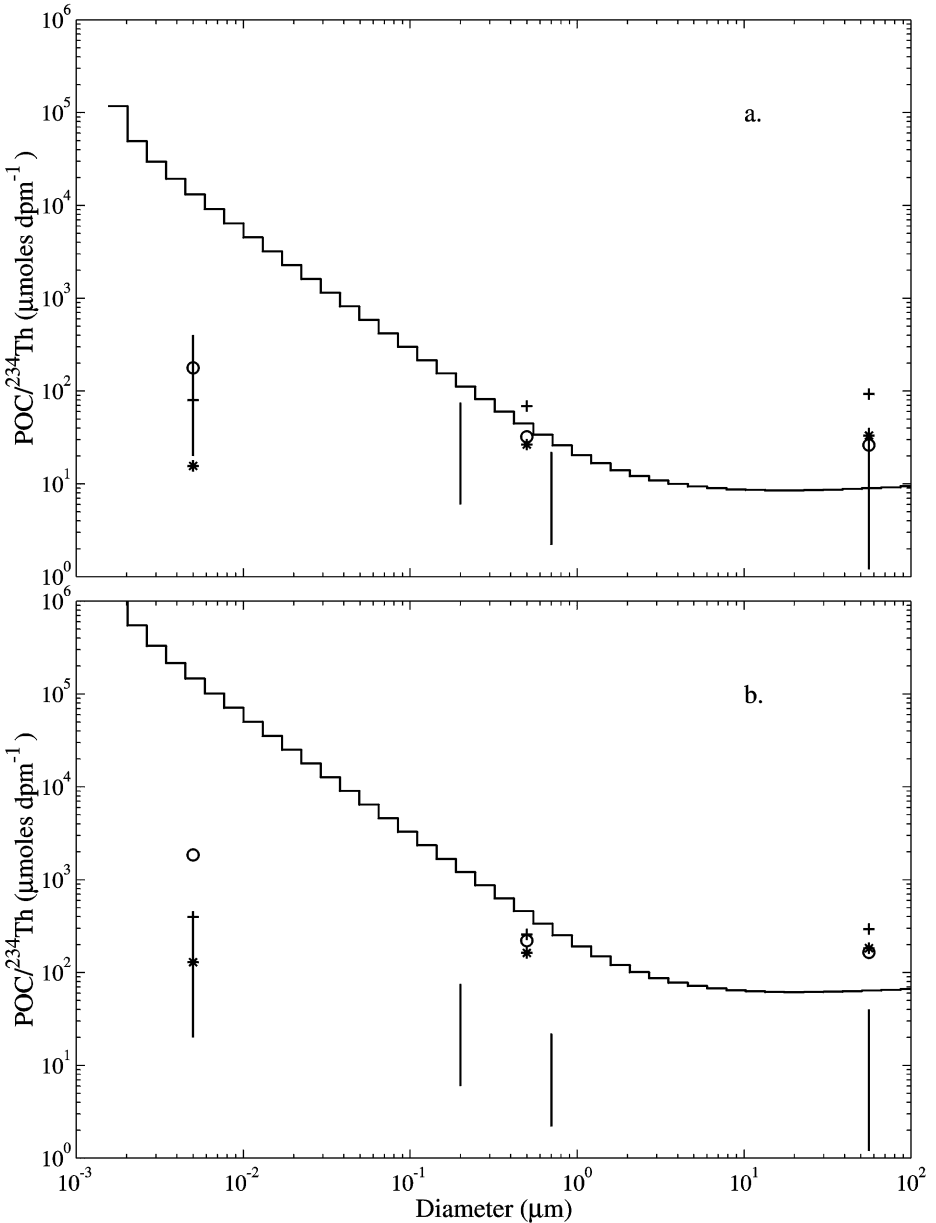


Fig. 5. Simulated  $POC/^{234}Th$  ratios for various model simulations using rectilinear kernels and a fractal dimension of 2.6. The vertical bars represent the ranges of the data shown in Fig. 1. The solid curve shows the simulation data for  $POC/^{234}Th$  using  $k_1^i = \text{constant}$  (model A). The dashed horizontal lines represent the particle size ranges used in comparing the simulated and observed data. The symbols correspond to the filtered data from the model for the various adsorption models: (○) adsorption model A ( $k_1^i = \text{constant}$ ); (\*) adsorption model B ( $k_1^i$  is transport-limited); (+) adsorption model C ( $k_1^i$  a mixture of constant and transport-limited). The two panels in the figure depict results from two simulations (a) particle input rate =  $0.01 \text{ mg l}^{-1} \text{ d}^{-1}$  and  $Z = 30 \text{ m}$ . (b) particle input rate =  $0.1 \text{ mg l}^{-1} \text{ d}^{-1}$  and  $Z = 3 \text{ m}$ .

much as three orders of magnitude greater than the observed values (Fig. 5b). However, such a direct comparison between the model output and the observations is misleading because the latter are obtained from filtrations. The act of filtration integrates the quantity of interest (e.g. the thorium activity) over the particle size distribution, which need not be uniform.

To make a meaningful comparison between the observed  $\text{POC}/^{234}\text{Th}$  ratios and the modeled values, the model results were integrated in such a way as to simulate a filtration experiment. To do this, three size classes were set up for the model results: colloids ( $d < 0.5 \mu\text{m}$ ), small particles ( $0.5 < d < 56 \mu\text{m}$ ) and large particles ( $d > 56 \mu\text{m}$ ). Several filter sizes were used in the observational data for small particles. For the simulation, a particle diameter of  $0.5 \mu\text{m}$  was chosen as being representative of this size class. Once the filter sizes were chosen, the particle size and thorium distributions were integrated over each size range determined by the filter sizes (Fig. 4).

The size distribution represented by the three size classes is much flatter than that given directly by the model. The values of the particulate organic carbon (Fig. 4a) and the particulate thorium (Fig. 4b) activity obtained by filtering are dominated by the peaks of the distribution within the size range. For the larger particles, the filtered value is dominated by those particles having sizes close to  $50 \mu\text{m}$ , and there is little indication of the rapid drop off in the particle distribution above about  $100 \mu\text{m}$ , and similarly for the colloidal particles, where the filtered value is dominated by particles close to  $0.5 \mu\text{m}$ .

$\text{POC}/^{234}\text{Th}$  ratios calculated from the filtered model results also show a decreasing trend with increasing particle size (open circles in Fig. 4c). For the colloidal particles, the filtered value is significantly lower in comparison to the unfiltered results. These filtered values are closer to the observed results (Fig. 5), though the agreement is better for the simulation having a thicker mixed layer depth and lower input rates. This may be due to increased biological interactions in the shallower regions.

Particles undergo disaggregation as well as aggregation. The model used in this work does not include disaggregation. Disaggregation models rely on parameters that are currently unknown or extremely hard to determine, such as the bond strengths holding the aggregate together. Sectional disaggregation models (Pandya and Spielman, 1982; Hill, 1996) require knowledge of the breakup probability as well as the size distribution of daughter particles. Jackson (1995) used a simplified disaggregation model when comparing model predictions with particle size distributions measured in a mesocosm. This model depended on two parameters, which were determined by comparing predicted and observed spectra using a least squares technique.

Trace metal adsorption models vary considerably in complexity (e.g., Bacon and Anderson, 1982; Clegg and Sarmiento, 1989). The model we used initially (model A) is one of the simplest, having the mass specific adsorption rate  $k^i$ , constant for particles of all sizes. Given the wide range of particle sizes used in the simulation ( $\sim 1 \text{ nm} - 100 \mu\text{m}$ ), one can ask how the value of  $k^i_1$  compares with transport rate of molecules to the particles. To answer this we made an explicit calculation of a size-dependent, transport-limited adsorption rate, with both advection and diffusion contributing to the transport of  $^{234}\text{Th}$  to the particles (model B). The adsorption rate

constant in this case was calculated using Eq. (18). For particles having a diameter greater than about 0.2  $\mu\text{m}$ , model A predicts an adsorption rate that is faster than the transport limited rate. This poses problems for scavenging models that use model A along with only two or three particle size classes. Such models often have adsorption only onto the small size class (e.g.,  $\sim 1\text{--}50\ \mu\text{m}$ ). Since the mass distribution typically has a broad peak in a similar size range (Fig. 4a), this is the particle size range that would have the fastest adsorption. However, it is precisely in this size range that the effects of transport limitation must be accounted for.

Results from the filtered models for all three adsorption models are shown in Fig. 5. Models B and C show a flatter distribution for the  $\text{POC}/^{234}\text{Th}$  ratio than mode A. For the small (0.5–56  $\mu\text{m}$ ) and large (> 56  $\mu\text{m}$ ) particles, all three models give approximately the same results. However for the colloidal particles, the adsorption rate for the transport limited case (model B) is larger than for models A and C, leading to a smaller  $\text{POC}/^{234}\text{Th}$  ratio.

Models and field data can be used together in many ways. Field data can be used to calibrate a model for a particular geographical region (Clegg and Whitfield, 1993). Field data and models can be combined to determine important parameters that are hard or impossible to measure (Murnane et al., 1996). In this work we attempted, as far as possible, to develop a model from first principles and compared the results we obtained with a collection of observational data. One reason for doing this is to gauge the complexity required of a model if it is to reproduce observed trends.

The model does reasonably well in predicting the trend of observed  $\text{POC}/^{234}\text{Th}$  with particle size. This implies that processes such as particle remineralization and biological interactions are probably secondary effects. They must however be included for a full understanding of thorium scavenging, particularly if the model is to be applied to geographically distinct regions and at different times.

Scavenging models are not traditionally based on detailed models of the particle size spectrum. The particle size spectrum plays a major role in the model used here. This increases the computational complexity of the model when compared to models that use only two or three particle size classes (e.g., Clegg and whitfield, 1993). The advantage of using this approach is that it allows size dependent effects to be examined with sufficient detail to rule out certain classes of models as being unphysical. Using only two or three particle size classes requires one to integrate quantities of interest over these classes, resulting in values that may be deceptive. This is because to obtain these, integrations are performed using a non-uniform particle size spectrum.

The lack of an explicit biological component in the model limits its use for non steady-state calculations. We are currently extending the model to include food-web dynamics. The model is also being developed in other directions. For example, the model deals with particle creation in a very idealized fashion: only colloidal particles with a radius of about 1 nm are input into the simulation, and all larger particles arise from coagulation of these monomers. In reality, marine particles have multiple sources and are extremely heterogeneous. Interactions between these various components are affected by the properties of the different particles (e.g., density, stickiness, size distribution). To predict these interactions successfully requires a model that is able to discriminate between different classes of particles as well as determine the

properties (e.g., the fractal dimension) of combinations of these particles as they aggregate. Non steady-state models have been applied to a mesocosm experiment (Jackson, 1995), where it was assumed that all aggregates were homogeneous. A model of heterogeneous systems has also been formulated (Jackson, 1998) using a two-dimensional particle size spectrum, though in this case the fractal dimensions of the two classes of particle were the same.

## Acknowledgements

We would like to acknowledge helpful discussions with Ken Buesseler and three reviewers whose comments helped to greatly improve the paper. Financial support for this work was provided by ONR to GAJ (N00014-87-K0005) and an ONR Young Investigator Award to SBM (N00014-96-1-0685).

## References

- Bacon, M.P., Anderson, R.F., 1982. Distribution of thorium isotopes between dissolved and particulate forms in the deep sea. *Journal of Geophysical Research* 87, 2045–2056.
- Bacon, M.P., Cochran, J.K., Hirschberg, D., Hammar, T.R., Fler, A.P., 1996. Export flux of carbon at the equator during the EqPac time-series cruises estimated from  $^{234}\text{Th}$  measurements. *Deep-Sea Research II* 43, 1133–1153.
- Baskaran, M., Santschi, P.H., Benoit, G., Honeyman, B.D., 1992. Scavenging of Thorium isotopes by colloids in seawater in the Gulf of Mexico. *Geochimica et Cosmochimica Acta* 56, 3375–3388.
- Buesseler, K.O., Andrews, J.A., Hartman, M.C., Belostock, R., Chai, F., 1995. Regional estimates of the export flux of particulate organic carbon derived from the thorium-234 during the JGOFS EqPac program. *Deep Sea Research II* 42, 777–804.
- Buesseler, K.O., Bacon, M.P., Cochran, J.K., Livingstone, H.D., 1992. Carbon and nitrogen export during the JGOFS North Atlantic Bloom Experiment estimated from the  $^{234}\text{Th}$ :  $^{238}\text{U}$  disequilibria. *Deep-Sea Research* 39, 1115–1137.
- Buesseler, K.O., Ball, L., Andrews, J.A., Belostock, R., Benitez-Nelson, C., 1996. Upper ocean particle export in the Arabian Sea. *Transactions, American Geophysical Union* 44, F396.
- Burd, A.B., Jackson, G.A., 1997. Predicting particle coagulation and sedimentation rates for a pulsed input. *Journal of Geophysical Research* 102, 10545–10561.
- Charette, M.A., Moran, S.B., 1999. Rates of particle scavenging and particulate organic carbon export estimated using  $^{234}\text{Th}$  as a tracer in the subtropical and equatorial Atlantic Ocean. *Deep-Sea Research II* in press.
- Charette, M.A., Moran, S.B., Bishop, J.K.B. 1999.  $^{234}\text{Th}$  as a tracer of particulate organic carbon export in the Subarctic Northeast Pacific Ocean, *Deep-Sea Research II* Submitted for publication.
- Clegg, S.L., Sarmiento, J.L., 1989. The hydrolytic scavenging of metal ions by marine particulate material. *Progress in Oceanography* 23, 1–21.
- Clegg, S.L., Whitfield, M., 1990. A generalized model for the scavenging of trace metals in the open ocean – I. particle cycling. *Deep-Sea Research* 37, 809–832.
- Clegg, S.L., Whitfield, M., 1993. Applications of a generalized scavenging model to time series  $^{234}\text{Th}$  and particle data obtained during the JGOFS North Atlantic Bloom Experiment. *Deep-Sea Research*. 40, 1529–1545.
- Clift, R., Grace, J.R., Weber, M.E., 1978. *Bubbles, Drops and Particles*. Academic Press, New York.
- Coale, K.H., Bruland, K.W., 1987. Oceanic stratified euphotic zone as elucidated by  $^{234}\text{Th}$ :  $^{238}\text{U}$  disequilibrium. *Limnology and Oceanography* 32, 189–200.

- Cochran, J.K., Barnes, C., Achman, D., Hirschberg, D.J., 1994. Thorium-234/Uranium-238 disequilibrium as an indicator of scavenging rates and particulate organic carbon fluxes in the NE Water Polynya, Greenland. *Journal of Geophysical Research* 100, 4399–4410.
- Drake, R.L., 1972. A general mathematical survey of the coagulation equation. In: Hidy, G.M., Brock, J.R. (Eds.), *Topics in Current Aerosol Research*. Pergamon, Tarrytown, N.Y., pp. 201–377.
- Farley, K.J., Morel, F.M.M., 1986. Role of coagulation in the kinetics of sedimentation. *Environmental Science and Technology* 20, 187–195.
- Gelbard, F., Tambour, Y., Seinfeld, J.H., 1980. Sectional representation for simulating aerosol dynamics. *Journal of Colloid and Interface Science* 76, 541–556.
- Hill, P.S., 1996. Sectional and discrete representations of floc breakage in agitated suspensions. *Deep-Sea Research I* 43, 679–702.
- Honeyman, B.D., Santschi, P.H., 1989. A Brownian-pumping model for oceanic trace metal scavenging: Evidence from Th isotopes. *Journal of Marine Research* 47, 951–992.
- Jackson, G.A., 1995. Comparing observed changes in particle size spectra with those predicted using coagulation theory. *Deep Sea Research II* 42, 159–184.
- Jackson, G.A., 1998. Using fractal scaling and two-dimensional particle size spectra to calculate coagulation rates for heterogeneous systems. *Journal of Colloid and Interface Science* 202, 20–29.
- Jackson, G.A., Lochmann, S., 1992. Effect of coagulation on nutrient and light limitation of an algal bloom. *Limnology and Oceanography* 37, 77–89.
- Jackson, G.A., Maffione, R., Costello, D.K., Alldredge, A.L., Logan, B.E., Dam, H.G., 1997. Particle size spectra between 1  $\mu\text{m}$  and 1 cm at Monterey Bay determined using multiple instruments. *Deep-Sea Research I* 44, 1739–1767.
- Jiang, Q., Logan, B.E., 1991. Fractal dimensions of aggregates determined from steady-state size distributions. *Environmental Science and Technology* 25, 2031–2038.
- Li, X., Logan, B.E., 1995. Size distributions and fractal properties of particles during a simulated phytoplankton bloom in a mesocosm. *Deep-Sea Research II* 42, 125–138.
- Li, X., Logan, B.E., 1997a. Collision frequencies between fractal aggregates and small particles in a turbulently sheared fluid. *Environmental Science Technology* 31, 1237–1242.
- Li, X., Logan, B.E., 1997b. Collision frequencies of fractal aggregates with small particles by differential sedimentation. *Environmental Science and Technology* 31, 1229–1236.
- Logan, B.E., Wilkinson, D.B., 1990. Fractal geometry of marine snow and other biological aggregates. *Limnology and Oceanography* 35, 130–136.
- Mann, K.H., Lazier, J.R.N., 1991. *Dynamics of Marine Ecosystems: Biological-Physical Interactions in the Oceans*. Blackwell, Oxford, UK.
- Moran, S.B., Buesseler, K.O., 1992. Short residence time of colloids in the upper ocean estimated from  $^{238}\text{U}$ – $^{234}\text{Th}$  disequilibria. *Nature* 359, 221–223.
- Moran, S.B., Buesseler, K.O., Niven, S.E.H., Bacon, M.P., Cochran, J.K., Livingston, H.D., Michaels, A.F., 1993. Regional variability in size-fractionated  $\text{C}/^{234}\text{Th}$  ratios in the upper ocean: importance of biological recycling. The Oceanography Society, Seattle, WA.
- Moran, S.B., Ellis, K.M., Smith, J.N. 1999. Distribution and export flux of  $^{234}\text{Th}$  and particulate organic carbon and nitrogen in the central Arctic Ocean. *Deep-Sea Research* submitted for publication.
- Murnane, R.J., Cochran, J.K., Buesseler, K.O., Bacon, M.P., 1996. Least-squares estimates of thorium, particle and nutrient cycling rate constants from the JGOFS North Atlantic Bloom Experiment. *Deep-Sea Research I* 43, 239–258.
- Murray, J.W., Young, J., Newton, J., Dunne, J., Chapin, T., Paul, B., McCarthy, J.J., 1996. Export flux of particulate organic carbon from the central equatorial Pacific determined using a combined drifting trap- $^{234}\text{Th}$  approach. *Deep Sea Research II* 43, 1095–1132.
- Niven, S.E.H., Kepkay, P.E., Boraie, A., 1995. Colloidal organic carbon and colloidal  $^{234}\text{Th}$  dynamics during a coastal phytoplankton bloom. *Deep-Sea Research II* 42, 257–273.
- Pandya, J.D., Spielman, L.A., 1982. Floc breakage in agitated suspensions: theory and data processing strategy. *Journal of Colloid and Interface Science* 90, 517–531.
- Peters, R.H., 1983. *The Ecological Implications of Body Size* Cambridge University Press, Cambridge.

- Press, W.H., Teukolsky, S.A., Vetterling, W.T., Flannery, B.P., 1992. Numerical Recipes in FORTRAN: The Art of Scientific Computing. Cambridge University Press, Cambridge.
- Pruppacher, H.R., Klett, J.D., 1980. Microphysics of Clouds and Precipitation. D. Reidel, Dordrecht.
- Smirnov, B.M., 1990. The properties of fractal clusters. Physics Reports 188, 1–78.
- Valiela, I., 1995. Marine Ecological Processes. 2nd Edition Springer, New York.
- Vicsek, T., 1992. Fractal Growth phenomena. 2nd Edition World Scientific, New Jersey.